Design of a resonator-bus-resonator anti-parity-time-symmetric integrated optical gyroscope

Design of a resonator-bus-resonator anti-parity-time-symmetric integrated optical gyroscope

Martino De Carlo[a], Francesco De Leonardis[a], Luciano Lamberti[b], Vittorio M. N. Passaro[a]

[a]*Photonics Research Group, Department of Electrical and Information Engineering, Politecnico di Bari, Via Orabona 4, Bari, 70126, Italy,*
[b]*Department of Mechanics, Mathematics and Management, Politecnico di Bari, Via Orabona 4, Bari, 70126, Italy,*

Abstract

Integrated optical gyroscopes are urgently required in different fields where space occupation and weight need to be minimized. However, in the state-of-the-art ring optical gyroscopes, Sagnac resonance splitting is proportional to the radius of the resonator, making it impossible to design an integrated gyroscope for high-resolution requirements. The enhancement of the sensitivity and the improvement in the limit of detection enabled by exceptional points has been already experimentally proved for parity-time-symmetric gyroscopes. Anti-parity-time-symmetric gyroscopes have been demonstrated to show even better performance, exhibiting a real eigenfrequency splitting, that can be easily measured. Here we present, for the first time, a resonator-bus-resonator anti-parity-time-symmetric integrated optical gyroscope designed on InP platform. This completely new architecture critically reduces the fabrication tolerance problems. The proposed configuration makes the gyroscope robust against the external perturbations that would make previous designs exit the anti-PT-symmetric condition. Moreover, this new architecture enables an electrical fine-tuning method for setting the system at the exceptional point. Finally, a time domain analysis is performed in this work, using the Fast Fourier Transform, to demonstrate the ease of its readout.

1. Introduction

The necessity of integrated optical gyroscopes for aerospace and consumer electronics applications is still an unsolved challenge. Ring laser gyroscopes

(RLGs) and interferometric fiber optic gyroscopes (IFOGs) are the commercial solutions for tactile grade gyroscopes. They are based on the relativistic Sagnac effect. However, the phase shift measured in RLGs and IFOGs, due to the Sagnac effect, is proportional to the linear dimensions of the device. This is why integrated optical gyroscopes are still an open challenge [1]. For applications where space and weight need to be reduced, as in aerospace or consumer electronics, an integrated solution is urgently required [2].

Khial et al. [3] have demonstrated an integrated nanophotonic optical gyroscope by exploiting the reciprocity of passive optical networks to reduce thermal fluctuations and mismatches. A 3-nrad phase shift has been identified between two counterpropagating optical beams on a 2-mm^2-footprint on silicon platform [3]. Thanks to several coils of silicon waveguides, Wu et al. [2] demonstrated a silicon integrated interferometric gyroscope with a sensitivity of 51.3 deg $/s$ on a footprint of 600 μm $\times$ 700μm. Long-range surface plasmon-polariton (LRSPP) active resonator has been theoretically predicted to have a sensitivity of 10^{-4} deg $/h$ [4].

However, the challenge for integrated gyroscopes for aerospace and consumer electronics applications is still open, requiring a new sensing principle, able to overcome the limitation of the Sagnac effect. Recently, non-Hermitian systems have been investigated in different fields for the interesting property of the enhanced sensitivity near their exceptional points. Since Bender et al. discovered that non-Hermitian Hamiltonians with parity-time (PT) symmetry have real spectra [5, 6], a lot of research has been carried out in optoelectronics [7], dealing with plasmonics [8], nanobeam cavities [9], whispering-gallery modes [10], coupled optical waveguides [11, 12], optomechanics [13, 14] and lasers at the exceptional point [15]. The advantage of exceptional points in PT-symmetric gyroscopes has been widely theoretically investigated [16, 17, 18, 19, 20]. The enhancement of spectral splitting due to mechanical rotation has been recently experimentally demonstrated on a Brillouin-based optical gyroscope working at the exceptional point [21] and on an RLG-based single-cavity parity-time-symmetric gyroscope [22]. In [23] the splitting between the eigenfrequencies of a PT-symmetric gyroscope has been shown to be complex [23], thus implying instability and difficulties in the readout. A valid alternative shown in [24] is the anti-parity-time-symmetric gyroscope, exhibiting a real splitting independent of the dimension of the device. The first anti-parity-time-symmetric gyroscope proposed in [24] needs high fabrication accuracy in the length of the U-shaped coupling waveguide, in order to keep the system at the exceptional point. Moreover, a relative

error on the optical length of the U-shaped waveguide (due to thermal fluctuation) would vanish all the advantages of anti-parity-time symmetry. The solution proposed in [24] requires high fabrication resolution and a feedback control on the U-shaped coupling bus in order to keep the system at the anti-PT-symmetric condition. In fact, the optical length of the two arms of the U-shaped waveguide are required to be an exact integer multiple of the design wavelength. However, on a length of several tens of microns, it is easy that a small relative error on that length or a small external perturbation could cause the coupling strength between the two cavities to become generally complex, thus exiting the anti-PT-symmetric condition. Due to the high sensitivity of exceptional points to external perturbations, minimizing the effect of all the parameters that could affect the exceptional point condition becomes a priority in the design of these devices.

Here we aim to overcome these problems, in order to make the system stable and easy to be implemented. Thanks to the use of one straight waveguide between two resonators, we can design an anti-parity-time symmetric gyroscope, much more stable and realistically implementable. Here we present a completely new architecture for anti-PT-symmetric optical sensors, also suitable for optical gyroscopes, and we show the design rules for its implementation on a standard InP platform. The solution here proposed will avoid any problem related to the constraints on the fabrication accuracy related to the length of the U-shaped auxiliary waveguide in [24]. Moreover, this new proposal will avoid the necessity of a feedback control on the optical length of that coupling waveguide. Finally, the solution proposed here will enable an external electrical control on the coupling strength between the two sensing resonators. As in the PT-symmetric gyroscopes, the lock-in effect is completely overcome thanks to the unidirectionality of light in the device.

2. Indirect-coupling anti-parity-time-symmetric optical systems

Parity-time-symmetric Hamiltonians have attracted attention in the field of optics for the interesting property of the phase transition at the exceptional points [10], which can be exploited for sensing applications. A generic system is PT-symmetric provided that its Hamiltonian $\hat{H}$ remains the same under the parity reflection (P) and the time reversal (T) operations ($PT\hat{H} = \hat{H}$), whereas an anti-PT-symmetric system complies with $PT\hat{H} = -\hat{H}$ [25]. An anti-PT-symmetric Hamiltonian for two coupled optical resonators is usually

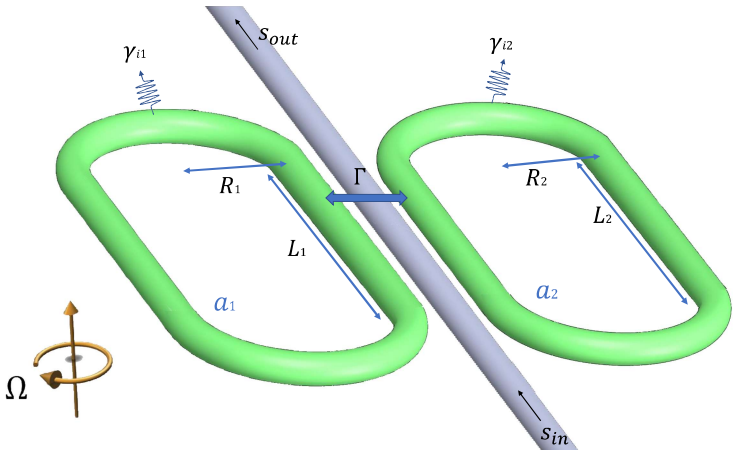

Figure 1: Indirect-coupling anti-parity-time-symmetric optical system.

written as:

$$\hat{H} = \begin{bmatrix} \frac{\omega_1-\omega_2}{2} - j\gamma' & -j\kappa \\ -j\kappa & \frac{\omega_2-\omega_1}{2} - j\gamma' \end{bmatrix} \tag{1}$$

where $\omega_{1,2}$ is the isolated resonance of the two resonators, γ' is the inverse of the photon lifetime in the ring and κ is the coupling strength between the two resonators. In order to satisfy the anticommutation relation ($PT\hat{H} = -\hat{H}$), the coupling strength, κ, needs to be a real value.

Recently, a configuration for an anti-parity-time symmetric-gyroscope has been proposed in [24], which requires an indirect coupling between optical resonators. The gyroscope in [24] shows some limitations due to fabrication tolerance constraints and the instability with respect to external perturbations. In fact, the solution for the indirect coupling proposed in [24] makes use of a U-shaped waveguide to couple two resonators. However, in such solution, the coupling strength, κ, is a function of the length of the U-shaped waveguide. Fabrication errors and mismatches between the length of the arms of the U-shaped waveguide could easily make the coupling strength non-real. Also temperature fluctuations would change the optical length of the auxiliary waveguide (influencing its effective index). This would cause the system to exit the anti-PT symmetric condition (non-real κ implies $PT\hat{H} \neq -\hat{H}$), vanishing all the advantages of exceptional points. Consequently, a feedback loop to control the phase of the optical path in the two arms of the U-shaped

waveguide would be necessary. Moreover, even in the presence of a feedback control, the phase of the coupling strength would still be wavelength dependent, allowing the anti-PT-symmetric condition to be achieved only at one single wavelength, thus worsening the sensitivity. In the present work we aim to design an indirectly-coupled-resonators anti-parity-time-symmetric optical gyroscope making use of only one auxiliary waveguide able to keep the anti-PT-symmetric condition without external feedback. With the proposed design, we can avoid any problem in terms of design and fabrication errors over the length of the auxiliary waveguides and be robust against external perturbations on the coupling strength. In order to achieve this goal, we propose the use of a resonator-bus-resonator coupler.

To demonstrate the feasibility of the device, we will show a solution compatible with the InP platform. The proposed device is shown in Figure 1, where s_{in} is the input signal, s_{out} is the output signal, $L_{1,2}$ is the length of the straight part of each racetrack resonator and $R_{1,2}$ is the radius of the bent part of the racetrack resonator, $\gamma_{i1,i2}$ is the inverse of the photon lifetime in each isolated resonator (net value of the intrinsic loss and the applied external gain) and Ω is the angular velocity of the frame of the device. Equation 2 describes the energy exchanges between the optical modes a_1 and a_2 inside the two resonators in the time domain [26, 27]:

$$\frac{d\boldsymbol{a}}{dt} = (j\boldsymbol{\omega} - \boldsymbol{\gamma_i} - \boldsymbol{\Gamma})\,\boldsymbol{a} + j\boldsymbol{\mu}^T s_{in} \tag{2}$$

$$s_{out} = s_{in} + j\boldsymbol{\mu}\boldsymbol{a} \tag{3}$$

with

$$\begin{aligned} \boldsymbol{a} = \begin{bmatrix} a_1 \\ a_2 \end{bmatrix}, \boldsymbol{\omega} = \begin{bmatrix} \omega_1 & 0 \\ 0 & \omega_2 \end{bmatrix}, \\ \boldsymbol{\gamma_i} = \begin{bmatrix} \gamma_{i1} & 0 \\ 0 & \gamma_{i2} \end{bmatrix}, \boldsymbol{\mu} = \begin{bmatrix} \mu_1 \\ \mu_2 \end{bmatrix}^T \end{aligned} \tag{4}$$

The term $\omega_{1,2}$ represents the resonance angular frequency of each isolated resonator, $\boldsymbol{\Gamma}$ is the decay rate matrix (it takes into account the energy exchange between the resonators and will be evaluated by using energy conservation observations), and $\mu_{1,2}$ is the coupling strength between the central bus and each resonator and can be evaluated as follows [28]:

$$\mu_{1,2}^2 = \frac{\eta_{1,2}^2 v_g}{P_{1,2}} \tag{5}$$

with $\eta_{1,2}^2$ the fraction of coupled power across the corresponding coupler and with $\mu_{1,2}$ a real positive term for two identical coupled waveguides.

As shown in [26] the terms $\boldsymbol{\mu}$ and $\boldsymbol{\Gamma}$ can be related using power conservation. Since the overall power is being conserved, we can evaluate $\boldsymbol{\Gamma}$, when all the other sources of loss are neglected and in the absence of input signal [26]:

$$\frac{d(\boldsymbol{a}^\dagger \boldsymbol{a})}{dt} + s_{out}^\dagger s_{out} = -2\boldsymbol{a}^\dagger \boldsymbol{\Gamma} \boldsymbol{a} + \boldsymbol{a}^\dagger \boldsymbol{\mu}^\dagger \boldsymbol{\mu} \boldsymbol{a} = 0 \tag{6}$$

where the symbol † represents the conjugate transpose. We can now obtain the expression of the matrix $\boldsymbol{\Gamma}$:

$$\boldsymbol{\Gamma} = \frac{1}{2}\boldsymbol{\mu}^\dagger \boldsymbol{\mu} = \frac{1}{2}\begin{bmatrix} \mu_1^2 & \mu_1\mu_2 \\ \mu_1\mu_2 & \mu_2^2 \end{bmatrix}, \tag{7}$$

After defining $\gamma'_{1,2} = \left(\gamma_{i,2} + \frac{\mu_{1,2}^2}{2}\right)$ and $\kappa = \mu_1\mu_2/2$, we can rewrite Eq. 2 as:

$$\frac{da_1}{dt} = j\omega_1 a_1 - \gamma'_1 a_1 - \kappa a_2 + j\mu_1 s_{in} \tag{8}$$

$$\frac{da_2}{dt} = j\omega_2 a_2 - \gamma'_2 a_2 - \kappa a_1 + j\mu_2 s_{in} \tag{9}$$

For $\omega_1 \neq \omega_2$, $\gamma' = \gamma'_1 = \gamma'_2$, after a simple variable change ($\tilde{a_{1,2}} = a_{1,2}e^{-j\omega_0 t}$, with $\omega_0 = (\omega_1 + \omega_2)/2$) the system is found to be anti-parity-time-symmetric, and we can use this device to design an anti-parity-time-symmetric gyroscope. We will continue to refer to equations 8 and 9, since the properties of the eigenfrequencies remains the same without the variable change.

Since the anti-parity-time-symmetric condition has been obtained starting from architectural considerations, without assumptions on the wavelength, it is a wavelength-independent condition.

So, we have been able to propose an anti-parity-time-symmetric optical system with a single auxiliary coupling waveguide (central bus), without any requirements on its length accuracy. While in [24] an error in the coupling

strength could easily make the system exit the anti-PT-symmetric condition ($PT\hat{H} \neq \hat{H}$), in this new architecture, the coupling strength is forced to be real by design. Moreover, differently from [24], the anti-PT-symmetric condition is achieved independently of the wavelength, (thus guaranteeing a better sensitivity).

3. Anti-PT-symmetric gyroscope

3.1. Eigenfrequency splitting

In order to evaluate the performances of the proposed device, we will evaluate the effect of the perturbation on the isolated resonances of the two resonators due to the rotation of the device. According to the Sagnac effect, the resonance frequency shift of a single isolated rotating optical resonator with respect to a rest condition is [29]:

$$\Delta\omega_{\Omega,i} = \pm\frac{4\pi A_i \Omega}{\lambda P_i n_{\text{eff}}} \tag{10}$$

where λ is the wavelength in vacuum, P_i and A_i are the perimeter and the enclosed area of the i-th resonator, n_{eff} is the effective index of the optical waveguides and Ω is the angular velocity of the frame.

The eigenfrequencies of the anti-PT-symmetric system described by Eqs. 8 and 9 are easily found to be:

$$\omega_{aPT_{1,2}} = \frac{\omega_1 + \omega_2}{2} + j\frac{\gamma_1' + \gamma_2'}{2} \pm \sqrt{\left(\frac{\omega_1 - \omega_2}{2}\right)^2 - \kappa^2}. \tag{11}$$

When the eigenfrequencies coalesce, the system is said to be at the exceptional point ($|\omega_1 - \omega_2| = 2\kappa$).

Since κ is a function of the wavelength, the condition of the exceptional point is rigorously verified only for a single wavelength. Practically, we need to verify Eq. 11 only at the central wavelength $\lambda_0 = 2\pi c/\omega_0$ (with c the speed of light). This can be experimentally achieved by fine-tuning the coupling strength κ (see paragraph 3.3).

If the system is designed to work around its exceptional point at rest condition ($\Omega = 0$), for $\Omega \neq 0$ the eigenfrequencies become:

$$\omega_{EP_{1,2}} = \frac{\omega_1 + \omega_2}{2} + j\gamma' \pm \sqrt{\kappa\Delta\omega_\Omega} \tag{12}$$

where

$$\Delta\omega_{\Omega} = \frac{4\pi\Omega}{\lambda n_{\text{eff}}}(A_1/P_1 + A_2/P_2) \tag{13}$$

Eq. 12 clarifies why it is necessary to have $\omega_1 \neq \omega_2$. In case of $\omega_1 = \omega_2$, it would be necessary to have $\kappa = 0$ to verify the condition of the exceptional point, leading to a null sensitivity (see Eq. 12). With $\omega_1 = \omega_2$, a degenerated case of an anti-PT-symmetry would be obtained instead, suitable for exceptional surface systems [30, 31].

Recalling from [28] that $\mu_{1,2}^2$ is proportional to the fraction of the power coupled from the bus to the ring ($\eta_{1,2}^2$) and to the inverse of the length of the cavity ($\mu_{1,2}^2 = \eta_{1,2}^2 \frac{v_g}{P_{1,2}}$), we can define the geometrical parameter:

$$\xi_i = \frac{A_i}{P_i^2} = \frac{2R_i/L_i + \pi(R_i/L_i)^2}{(2\pi R_i/L_i + 2)^2} \tag{14}$$

with R_i and L_i the radius of curvature and the length of the straight waveguide of the racetrack resonator (see Figure 1). Starting from Eq. 13 and using Eq. 14 and Eq. 5, we can obtain:

$$\Delta\omega_{EP} \approx \sqrt{\frac{4\pi\eta_1\eta_2 v_g}{\lambda n_{\text{eff}}}\xi\Omega} \tag{15}$$

where $\xi = \xi_1 \approx \xi_2$ (in the realistic hypotheses of $A_1 \approx A_2$ and $P_1 \approx P_2$).

As in the PT-symmetric gyroscope in [23] and in the anti-PT-symmetric gyroscope in [24], the eigenfrequency splitting has been demonstrated to be independent of the area occupied by the device, once the shape has been fixed (constant ratio R_i/L_i, corresponding to a fixed value of ξ) and for fixed values of η_1 and η_2. In this way, the limitation of the Sagnac splitting is overcome. As in the PT-symmetric case, the splitting is proportional to $\sqrt{\Omega}$, thus leading to enhanced sensitivity in the proximity of the exceptional point.

3.2. Stability, noise and detectivity

In this paragraph we want to underline that the proposed anti-PT-symmetric gyroscope has the important advantage over the PT-symmetric counterpart of exhibiting a real splitting, differently from the complex splitting in the PT-symmetric gyroscope ($\Delta\omega_{PT,EP} = (1+j)\sqrt{\kappa\Delta\omega_{\Omega}}$, with κ the direct coupling strength between the two resonators [23]). The real splitting of the anti-PT-symmetric gyroscope can be easily read through the beating frequency at the output of the photoreceiver. The real splitting has an important consequence

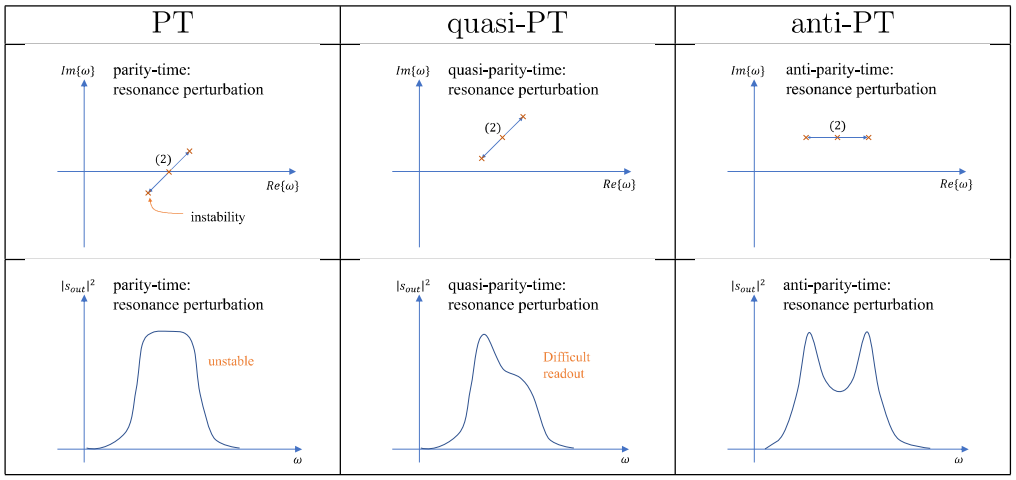

Table 1: PT vs quasi-PT vs anti-PT analysis

on the stability analysis, as it has been already demonstrated in [32]. In order to analyze the stability of the proposed gyroscope, we need to perform a time-domain analysis. The time behavior of the modes in the cavities is easily found in the time domain, by using the eigenfrequencies in Eq. 12 [33]:

$$a_{1,2} \approx e^{j\omega_{EP_{1,2}}} = e^{j\left(\frac{\omega_1+\omega_2}{2} \pm \sqrt{\kappa\Delta\omega_\Omega}\right)t} e^{-\gamma' t} \tag{16}$$

these two modes are both stable (for a positive value of $\Delta\omega_\Omega$), because real part of the argument of the exponential term is negative. For the opposite sense of rotation (negative value of $\Delta\omega_\Omega$), it would be sufficient to invert the input and the output signals, in order to prevent instability.

Whereas, in the PT-symmetric case,

$$a_{1,2_{PT}} \approx e^{j\omega_{PT,EP_{1,2}}} = e^{j\omega_0} e^{\pm\sqrt{\kappa\Delta\omega_\Omega}}, \tag{17}$$

the square root term leads to a divergent mode, making the system always unstable. A possible solution to this problem would be to make the system quasi-PT-symmetric, with a negative average gain of the resonators ($\gamma_1' + \gamma_2' < 0$), by adding a common loss to both the resonators. However, since the eigenfrequency splitting is complex, the readout system would be difficult as shown in [32] (see Table 1).

The performed stability analysis has an important consequence on the noise influence on the sensor. A small perturbation, for example noise, applied to any of the parameters of the PT-symmetric gyroscope has drastic

consequences on the stability of the system, even in unperturbed conditions. In fact, noise would easily make one of the eigenfrequencies cross the real frequency axis, thus leading to instability as shown in [34]. In this perspective, the superiority of the anti-PT-symmetric gyroscope with respect to the PT-counterpart is also related to the distance of the eigenfrequencies of the anti-PT-symmetric systems from the real axis of frequency.

A well-known drawback of exceptional-point based sensors is represented by the accuracy necessary for approaching the exceptional point [34]. It is easy to show that if the system is not exactly at the exceptional point at rest condition, Eq. 12 holds until the perturbation to be sensed is much higher than the error in the exceptional point condition (δ_{EP}):

$$\delta_{EP} = \left| \left(\frac{\omega_1 - \omega_2}{2} \right)^2 + \kappa^2 \right| << \left| \kappa \Delta\omega_\Omega \right| . \tag{18}$$

The minimum detectable angular velocity should satisfy the condition in Eq. 18. So, we can give an estimation of the minimum detectable angular velocity by considering the right term of the inequality in Eq. 18 ten times greater than δ_{EP}, leading to:

$$\Omega_{min} \approx \frac{5 n_{\text{eff}} n_g}{\omega_0 \eta_1 \eta_2 \xi} \delta_{EP}. \tag{19}$$

In this perspective, in exceptional-point-based sensors the detectivity is determined by the resolution of a feedback loop in controlling the isolated resonances of the resonators (ω_1 and ω_2) or the coupling strength (κ). We want to underline that in this architecture κ is forced to be a real value, thus making it necessary only to have one feedback control on its absolute value (shown in the next paragraph). Whereas, in [24] two simultaneous feedback controls, both on the phase and on the absolute value of the coupling strength, are necessary.

3.3. Coupling strength control

We want to underline that, using a single straight waveguide (central bus) to couple two resonators has an important advantage. When using the U-shaped configuration [24] or two coupling waveguides [35], an error on the length of the coupling waveguides could not only increase the difficulty in approaching the exceptional point condition (worsening the detectivity of the device), but could also cause the coupling strength and, consequently,

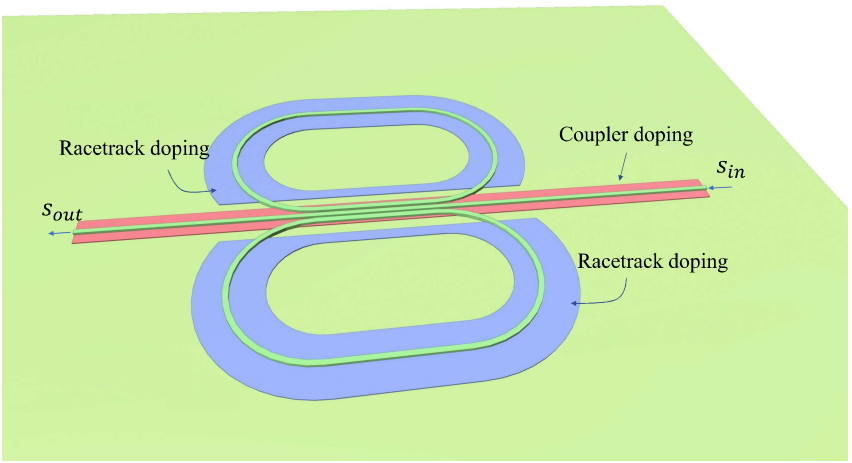

Figure 2: Design proposal for an optical anti-parity-time-symmetric optical gyroscope on InP platform.

the eigenfrequency splitting to become generically complex, thus denying the anti-PT symmetry. The resonator-bus-resonator coupler ensures much more reliability and control over the coupling strength of the system, by keeping the value of κ^2 real. Moreover, the proposed structure enables an easy way to electrically fine tune the system around the exceptional point, through the control of the loss/gain in the coupling region and the consequent variation of the coupling strength.

In the previous paragraph the coupling mechanism has been supposed to be lossless, however, when considering a lossy (or with gain) coupler, an additional source of loss (or gain, with negative sign) should be accounted in $\gamma'_{1,2}$

$$\gamma'_{1,2} = \left(\gamma_{i,2} + \frac{\mu^2_{add,1,2}}{2} + \frac{\mu^2_{1,2}}{2}\right) \tag{20}$$

where:

$$\mu^2_{add_{1,2}} = \frac{\chi^2_{1,2} v_g}{(2\pi R_{1,2})} \tag{21}$$

with $\chi^2_{1,2}$ the fraction of power lost in the coupling region,

3.4. Readout

The device output can be read using both wavelength interrogation and amplitude interrogation. In the first case, a narrow-linewidth laser should be used as input and a photoreceiver to read the output s_{out}. Simple electronics can be used to process the output and read the splitting, from the optical spectrum. Instead, for the amplitude interrogation, a broadband source (sufficiently broad to cover the range of wavelengths of interest around the central angular frequency ω_0, but not the adjacent central resonances) can be used as input. In particular, reading a photoreceiver at the output port would generate a photocurrent proportional to the incident optical power. By approximating the two peaks of the output response as two perfect sine curves at angular frequencies $\omega_{EP,1}$ and $\omega_{EP,2}$, and considering the effect of a photoreceiver as a low pass filtering of the optical power, we obtain a cosine at angular frequency $\omega_{EP,1} - \omega_{EP,2}$ in the electrical signal generated at the photodetector:

$$[sin(\omega_{EP,1}t) + sin(\omega_{EP,2}t)]^2 \xrightarrow{\text{LPF}} cos[(\omega_{EP,1} - \omega_{EP,2})t]. \tag{22}$$

A careful reader could have noticed that the frequency splitting in Eq. 12 is real only when $\Delta\omega_\Omega$ is positive (corresponding to an angular velocity that increases ω_1 and decreases ω_2). When the gyroscope is rotating in the opposite direction, $\Delta\omega_\Omega$ becomes negative and the splitting is imaginary and the splitting is not appreciable on the output spectrum anymore. In this case, making the light flow into the device in the opposite direction would make $\Delta\omega_\Omega$ positive again. So, injecting the input signal at the output port, and reading the output at the input port, would make it possible to detect angular velocities in the opposite direction, as well. By redirecting light in opposite directions in the device at a frequency much faster than $\Delta\omega_\Omega$ could be helpful to detect both positive and negative angular velocities.

4. Design and results

In this section, we show our proposal for integrating the anti-parity-time-symmetric gyroscope on an InP platform. The proposed architecture is shown in Fig. 2 and will be explained in the following paragraphs.

4.1. Cross-section design

Here we list the material composition and the thickness of each layer of the cross-section in Fig. 3a (where the symbols in brackets represent the

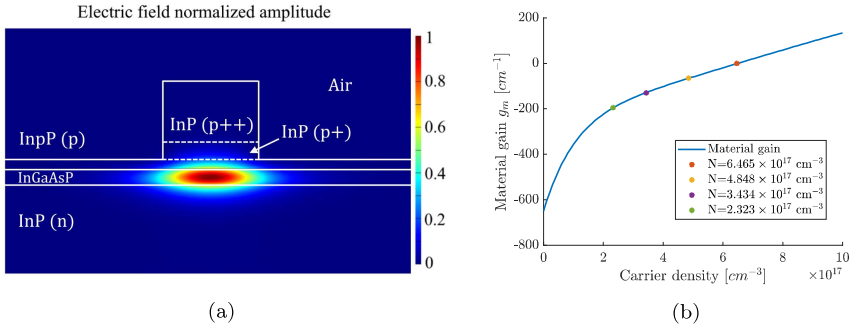

(a) (b)

Figure 3: (a) Normalized electric field and cross-section of the waveguide adopted in all the regions of the integrated gyroscope. (b) Material gain of InGaAsP as a function of the density of the injected carriers, obtained with the model in [37]. The marked dots in the legend represent the values of the carrier density, used in the design of the coupler.

type of doping), with the corresponding p-type (p) or n-type (n) doping concentration and material refractive index (RI):

- InP-p (1000 nm, $p = 1.5 \times 10^{18}$ cm^{-3}, RI = 3.17)
- InP-p (250 nm, $p = 8 \times 10^{17}$ cm^{-3}, RI = 3.17)
- InP-p (150 nm, $p = 5 \times 10^{17}$ cm^{-3}, RI = 3.17)
- $In_{0.6}Ga_{0.4}As_{0.85}P_{0.15}$ (250 nm, RI = 3.50 [36])
- InP-n (1000 nm, $n = 1 \times 10^{18}$ cm^{-3}, RI = 3.17)

The material gain of the InGaAsP has been evaluated using the semi-empirical model proposed in [37], using the parameters used in the simulation tool (Table I of [37]). The predicted material gain as a function of the carrier density for a wavelength of 1.55 μm is shown in Figure 3b. The material gain has been converted into the extinction coefficient (k, imaginary part of the refractive index) of the gain region of the cross-section according to the relation ($k = g_m\lambda/4\pi$). This value has been used for the simulation of the coupler. Once the confinement factor $\Gamma_g = 55,59\%$ has been evaluated, the net gain can be calculated as $\gamma_i = -\Gamma_g g_m$ (by considering the other materials as lossless).

Figure 3a shows the cross-section of the InP waveguide, common to all the waveguides and the resonators of the designed gyroscope, including the central coupling waveguide. The width of the rib is 1.5 μm.

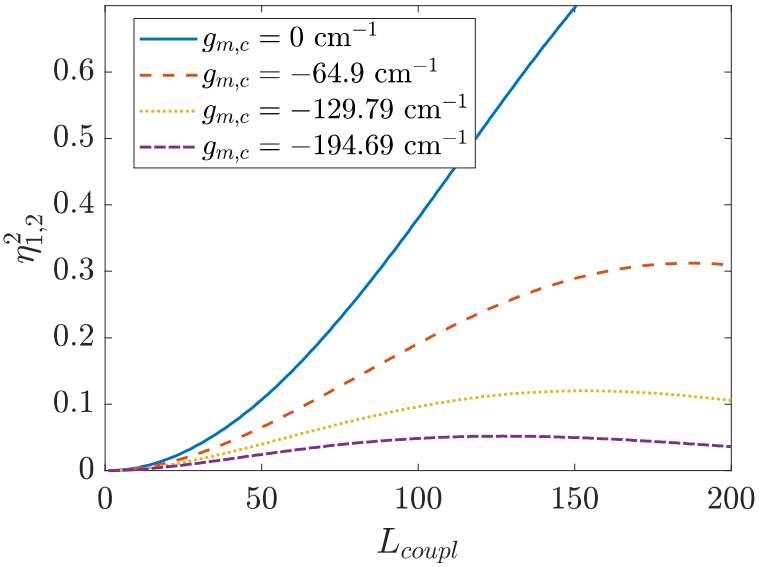

Figure 4: Coupling efficiency $\eta_{1,2}$ for different values of the material gain of the InGaAsP coupling region ($g_{m,c}$), corresponding to the carrier density N marked in Fig. 3b.

4.2. Coupler design

After that, we designed the coupling region with a propagator software. The gap between the edges of the rib has been set to 1 μm. The value of $\eta_{1,2}$ can be obtained by evaluating the fraction of power coupled from the racetrack to the auxiliary waveguide (same in the opposite direction). After that, Eq. 5 can be used to compute $\mu_{1,2}$. It should be noted that the coupling region can be electrically isolated from the rest of the device (by means of an undoped region in between), in order to make it possible to control the coupling strength by tuning the gain in the coupling region, separately from the gain of the two resonators (Figure 2). In fact, by controlling the gain in the coupling region, while compensating the losses of the InGaAsP material, it is possible to control the quantity $\eta_{1,2}$. Figure 4 shows the coupling power coefficient for different carrier injection level in the coupling region, varying with the length of the straight coupling region.

According to simulations, for a InGaAsP material gain ranging from -194.69 to 0 cm^{-1} (corresponding to a carrier injection ranging from 2.323×10^{17} to 6.465×10^{17} cm^{-3}, see Fig. 3b), the coupled power fraction at $L_1 = L_2 = 120\mu m$ goes from less than 5% to 51%. This means having a wide range

of tunability for κ. The value of the gain is negative, because we only use carrier injection to partially compensate the losses due to absorption up to the transparency condition. The cross-sections of the waveguides have been designed in order to keep the cross coupling from the waveguide of the first ring and the waveguide of the second ring at least two orders of magnitude lower than the direct coupling of both the waveguides with the central one.

4.3. Gyroscope design

For evaluating the performances of the device, we designed it at the exceptional point. The values chosen for the simulations are summarized in Table 2.

Parameter	Value
n_{eff}	3.268
R_1	50μm
R_2	50.6μm
L_1	120μm
L_2	120μm
γ'_1	5×10^4 rad/s
γ'_2	5×10^4 rad/s

Table 2: Parameters used in the simulations

In particular, once the isolated eigenfrequencies ω_1 and ω_2 have been calculated, by using the effective index (value in Table 2) and the lengths of the perimeters of the racetracks ($P_{1,2} = 2\pi R_{1,2} + 2L_{1,2}$), the coupling strength κ has been designed as:

$$\kappa = |\omega_1 - \omega_2|/2 \tag{23}$$

Once the value of κ has been obtained ($\kappa \approx 3.15 \times 10^{10}$ rad/s), it is possible to evaluate μ_1 and μ_2, using Eq. 5, recalling that $\kappa = \mu_1\mu_2/2$, with the assumption $\eta_1 = \eta_2$ (symmetrical coupler). We obtained $\mu_1 \approx 2.515 \times 10^5 (rad/s)^{1/2}$ and $\mu_2 \approx 2.506 \times 10^5 (rad/s)^{1/2}$ ($\eta_{1,2}^2 \approx 0.3818$).

It could be helpful to estimate the internal gain of the resonators ($-\gamma'_{i,1,2}$), although they will be experimentally tuned with a feedback control on the resonance linewidth. Using the value of $\gamma'_{1,2}$ in Table 2, neglecting $\mu^2_{add,1,2}/2$ (since the coupler is designed near transparency), and using the calculated values for μ_1 and μ_2, we obtain $\gamma_{i,1} = -3.1622 \times 10^{10}$ rad/s and

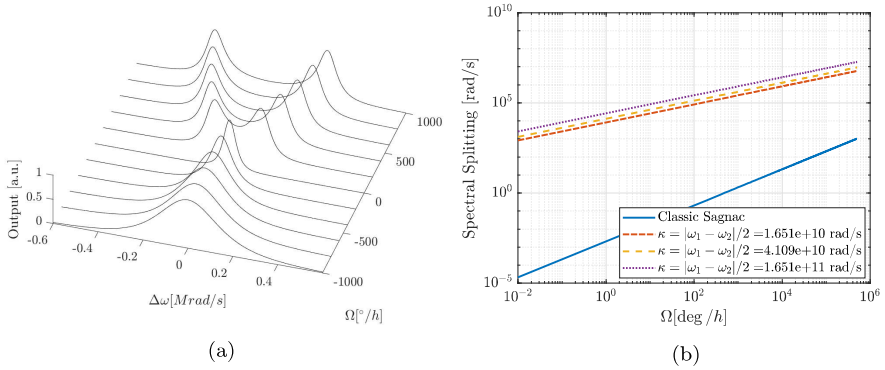

(a) (b)

Figure 5: (a) Spectrum of the output signal of the gyroscope as a function of the angular velocity and of the frequency detuning from ω_0. (b) Splitting as a function of the angular velocity

$\gamma_{i,2} = -3.1408 \times 10^{10}$ rad/s, corresponding to power gains per length of 6.89 cm^{-1} and 6.84 cm^{-1}, respectively. It should be noted that these values are approximated, arising from a simplified model. They should be helpful in the design of the device, but the external experimental tuning would be important to place the device at the exceptional point.

The results of the output spectrum ($|s_{out}|^2$) are shown in Figure 5a. Figure 5b shows the eigenfrequency splitting as a function of the angular velocity of the proposed anti-PT-symmetric gyroscope compared to the classical Sagnac splitting on a single resonator of the same dimensions of one of the designed resonators. The performance obtained with the new proposed resonator-bus-resonator configuration is comparable with that obtained in [24]. In fact, equations 8-9 are formally equivalent to those describing the anti-PT-symmetric gyroscope in [24]. So, provided that the coupling strengths are the same, the same sensitivity can be achieved, with an enormous advantage from the fabrication point of view, and for the stability with respect to external perturbations.

Finally, figures 6a and 6b show the time behavior of output optical power $|s_{out}|^2$ read at a photodetector for a pulsed input s_{in}. In particular, a Gaussian pulse modulating an optical carrier at an angular frequency ω_0 has been simulated, with a standard deviation of 1 μs and with the peak of the pulse centered at $t = 1.8$ μs. In this way, it is easy to appreciate that the system is stable and that it would be possible to extract the angular velocity of the gyroscope using some basic signal processing. The two graphs have been ob-

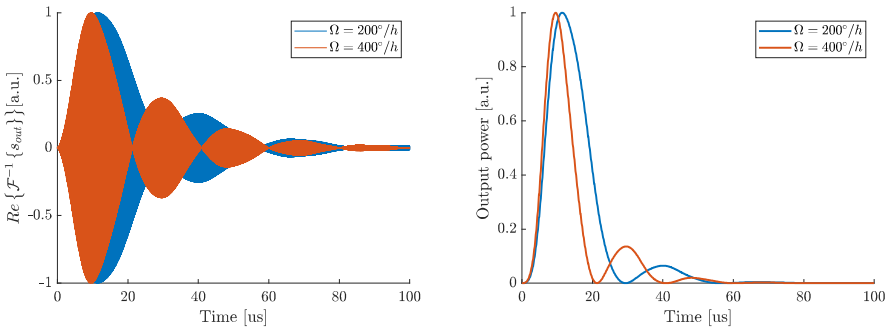

(a) (b)

Figure 6: (a) Normalized real part of the output signal s_{out} in the time domain for an input Gaussian pulse s_{in}. (b) Normalized $|s_{out}|^2$ in the time domain for an input Gaussian pulse s_{in}, representing the average optical power at the photoreceiver.

tained as the real part and the squared absolute value of the inverse Fourier Fast Transformation of the output signal.

5. Conclusions

We showed a new architecture for an anti-PT-symmetric integrated optical gyroscope. The gyroscope is realized using two resonators, indirectly coupled by means of one straight auxiliary waveguide. With respect to the previously proposed anti-PT-symmetric gyroscope, the use of only one auxiliary waveguide (central bus) makes the anti-PT-symmetric condition robust against external perturbations and verified for a wide range of wavelengths. Moreover, the sensitivity of the gyroscope has been demonstrated to be independent of the dimensions of the device, even for racetrack resonators. Such a conclusion represents noticeable progress with respect to the classical Sagnac effect, limited by the dependence of the sensitivity on the radius of the ring resonator.

As a result, the device shows an incredibly enhanced sensitivity with respect to the classical Sagnac effect on a device of the same dimensions: the sensitivity of an anti-PT-symmetric micrometric gyroscope could be several orders of magnitude higher than a classical Sagnac gyroscope.

Our solution seems to be much more suitable for angular velocity sensing than the PT-symmetric gyroscope. In fact, the anti-PT-symmetric gyroscope exhibits a real resonance splitting, with respect to the PT-symmetric

one. We showed that the anti-PT-symmetric is a suitable configuration for a stable gyroscope with a simple readout, whereas making a PT-symmetric gyroscope stable would cause difficulties in the electronic readout. Finally, we believe that the device we modeled could pave the way to a new generation of integrated optical gyroscopes, breaking the limit of micrometric dimensions.

References

[1] V. M. N. Passaro, A. Cuccovillo, L. Vaiani, M. De Carlo, and C. E. Campanella, "Gyroscope technology and applications: A review in the industrial perspective," *Sensors*, vol. 17, no. 10, p. 2284, Oct. 2017. [Online]. Available: https://doi.org/10.3390/s17102284

[2] B. Wu, Y. Yu, J. Xiong, and X. Zhang, "Silicon integrated interferometric optical gyroscope," *Scientific Reports*, vol. 8, no. 1, jun 2018. [Online]. Available: https://doi.org/10.1038/s41598-018-27077-x

[3] P. P. Khial, A. D. White, and A. Hajimiri, "Nanophotonic optical gyroscope with reciprocal sensitivity enhancement," *Nature Photonics*, vol. 12, no. 11, pp. 671–675, oct 2018. [Online]. Available: https://doi.org/10.1038/s41566-018-0266-5

[4] T. Zhang, G. Qian, Y.-Y. Wang, X.-J. Xue, F. Shan, R.-Z. Li, J.-Y. Wu, and X.-Y. Zhang, "Integrated optical gyroscope using active long-range surface plasmon-polariton waveguide resonator," *Scientific Reports*, vol. 4, no. 1, Jan. 2014. [Online]. Available: https://doi.org/10.1038/srep03855

[5] C. M. Bender and S. Boettcher, "Real spectra in non-hermitian hamiltonians Having PT Symmetry," *Physical Review Letters*, vol. 80, no. 24, pp. 5243–5246, Jun. 1998. [Online]. Available: https://doi.org/10.1103/physrevlett.80.5243

[6] C. M. Bender, S. Boettcher, and P. N. Meisinger, "PT-symmetric quantum mechanics," *Journal of Mathematical Physics*, vol. 40, no. 5, pp. 2201–2229, May 1999. [Online]. Available: https://doi.org/10.1063/1.532860

[7] C. E. Rüter, K. G. Makris, R. El-Ganainy, D. N. Christodoulides, M. Segev, and D. Kip, "Observation of parity–time symmetry in optics," *Nature Physics*, vol. 6, no. 3, pp. 192–195, Jan. 2010. [Online]. Available: https://doi.org/10.1038/nphys1515

[8] H. Benisty, A. Degiron, A. Lupu, A. D. Lustrac, S. Chénais, S. Forget, M. Besbes, G. Barbillon, A. Bruyant, S. Blaize, and G. Lérondel, "Implementation of PT symmetric devices using plasmonics: principle and applications," *Optics Express*, vol. 19, no. 19, p. 18004, Aug. 2011. [Online]. Available: https://doi.org/10.1364/oe.19.018004

[9] S. Zhang, Z. Yong, Y. Zhang, and S. He, "Parity-time symmetry breaking in coupled nanobeam cavities," *Scientific Reports*, vol. 6, no. 1, Apr. 2016. [Online]. Available: https://doi.org/10.1038/srep24487

[10] B. Peng, Ş. K. Özdemir, F. Lei, F. Monifi, M. Gianfreda, G. L. Long, S. Fan, F. Nori, C. M. Bender, and L. Yang, "Parity–time-symmetric whispering-gallery microcavities," *Nature Physics*, vol. 10, no. 5, pp. 394–398, Apr. 2014. [Online]. Available: https://doi.org/10.1038/nphys2927

[11] S. Klaiman, U. Günther, and N. Moiseyev, "Visualization of branch points in pt-symmetric waveguides," *Physical Review Letters*, vol. 101, no. 8, Aug. 2008. [Online]. Available: https://doi.org/10.1103/physrevlett.101.080402

[12] A. Guo, G. J. Salamo, D. Duchesne, R. Morandotti, M. Volatier-Ravat, V. Aimez, G. A. Siviloglou, and D. N. Christodoulides, "Observation of pt-symmetry breaking in complex optical potentials," *Physical Review Letters*, vol. 103, no. 9, Aug. 2009. [Online]. Available: https://doi.org/10.1103/physrevlett.103.093902

[13] W. Li, Y. Jiang, C. Li, and H. Song, "Parity-time-symmetry enhanced optomechanically-induced-transparency," *Scientific Reports*, vol. 6, no. 1, Aug. 2016. [Online]. Available: https://doi.org/10.1038/srep31095

[14] M. De Carlo, F. De Leonardis, L. Lamberti, and V. M. N. Passaro, "Generalized modeling of optomechanical forces applied to PT-symmetric optical microscale resonators," *Journal of Lightwave*

Technology, vol. 37, no. 10, pp. 2178–2184, May 2019. [Online]. Available: https://doi.org/10.1109/jlt.2019.2899486

[15] M. Brandstetter, M. Liertzer, C. Deutsch, P. Klang, J. Schöberl, H. E. Türeci, G. Strasser, K. Unterrainer, and S. Rotter, "Reversing the pump dependence of a laser at an exceptional point," *Nature Communications*, vol. 5, no. 1, Jun. 2014. [Online]. Available: https://doi.org/10.1038/ncomms5034

[16] S. Sunada, "Large sagnac frequency splitting in a ring resonator operating at an exceptional point," *Physical Review A*, vol. 96, no. 3, Sep. 2017. [Online]. Available: https://doi.org/10.1103/physreva.96.033842

[17] M. J. Grant and M. J. F. Digonnet, "Loss-gain coupled ring resonator gyroscope," in *Optical, Opto-Atomic, and Entanglement-Enhanced Precision Metrology*, S. M. Shahriar and J. Scheuer, Eds. SPIE, Mar. 2019. [Online]. Available: https://doi.org/10.1117/12.2515657

[18] D. D. Smith, H. Chang, L. Horstman, and J.-C. Diels, "Parity-time-symmetry-breaking gyroscopes: lasing without gain and subthreshold regimes," *Optics Express*, vol. 27, no. 23, p. 34169, Nov. 2019. [Online]. Available: https://doi.org/10.1364/oe.27.034169

[19] S. Jiang, X. Chang, W. Li, P. Han, Y. Zhou, H. Zhang, A. Huang, and Z. Xiao, "On-chip high sensitivity rotation sensing based on higher-order exceptional points," *Journal of the Optical Society of America B*, vol. 36, no. 9, p. 2618, Aug. 2019. [Online]. Available: https://doi.org/10.1364/josab.36.002618

[20] L. Horstman, N. Hsu, J. Hendrie, D. Smith, and J.-C. Diels, "Exceptional points and the ring laser gyroscope," *Photonics Research*, vol. 8, no. 3, p. 252, Feb. 2020. [Online]. Available: https://doi.org/10.1364/prj.369521

[21] Y.-H. Lai, Y.-K. Lu, M.-G. Suh, Z. Yuan, and K. Vahala, "Observation of the exceptional-point-enhanced sagnac effect," *Nature*, vol. 576, no. 7785, pp. 65–69, Dec. 2019. [Online]. Available: https://doi.org/10.1038/s41586-019-1777-z

[22] M. P. Hokmabadi, A. Schumer, D. N. Christodoulides, and M. Khajavikhan, "Non-hermitian ring laser gyroscopes with enhanced

sagnac sensitivity," *Nature*, vol. 576, no. 7785, pp. 70–74, Dec. 2019. [Online]. Available: https://doi.org/10.1038/s41586-019-1780-4

[23] M. De Carlo, F. De Leonardis, and V. M. N. Passaro, "Design rules of a microscale PT-symmetric optical gyroscope using group IV platform," *Journal of Lightwave Technology*, vol. 36, no. 16, pp. 3261–3268, Aug. 2018. [Online]. Available: https://doi.org/10.1109/jlt.2018.2837754

[24] M. De Carlo, F. D. Leonardis, L. Lamberti, and V. M. N. Passaro, "High-sensitivity real-splitting anti-PT-symmetric microscale optical gyroscope," *Optics Letters*, vol. 44, no. 16, p. 3956, Aug. 2019. [Online]. Available: https://doi.org/10.1364/ol.44.003956

[25] Y. Choi, C. Hahn, J. W. Yoon, and S. H. Song, "Observation of an anti-PT-symmetric exceptional point and energy-difference conserving dynamics in electrical circuit resonators," *Nature Communications*, vol. 9, no. 1, jun 2018. [Online]. Available: https://doi.org/10.1038/s41467-018-04690-y

[26] Y. Zhang, T. Mei, and D. H. Zhang, "Temporal coupled-mode theory of ring–bus–ring mach–zehnder interferometer," *Applied Optics*, vol. 51, no. 4, p. 504, Jan. 2012. [Online]. Available: https://doi.org/10.1364/ao.51.000504

[27] S. Fan, W. Suh, and J. D. Joannopoulos, "Temporal coupled-mode theory for the fano resonance in optical resonators," *Journal of the Optical Society of America A*, vol. 20, no. 3, p. 569, Mar. 2003. [Online]. Available: https://doi.org/10.1364/josaa.20.000569

[28] B. E. Little, S. T. Chu, H. A. Haus, J. Foresi, and J. . Laine, "Microring resonator channel dropping filters," *Journal of Lightwave Technology*, vol. 15, no. 6, pp. 998–1005, June 1997.

[29] G. B. Malykin, "Sagnac effect in ring lasers and ring resonators. how does the refractive index of the optical medium influence the sensitivity to rotation?" *Physics-Uspekhi*, vol. 57, no. 7, pp. 714–720, Jul. 2014. [Online]. Available: https://doi.org/10.3367/ufne.0184.201407g.0775

[30] Q. Zhong, J. Ren, M. Khajavikhan, D. Christodoulides, Ş. Özdemir, and R. El-Ganainy, "Sensing with exceptional surfaces in order to combine sensitivity with robustness," *Physical Review*

Letters, vol. 122, no. 15, Apr. 2019. [Online]. Available: https://doi.org/10.1103/physrevlett.122.153902

[31] M. De Carlo, F. De Leonardis, R. A. Soref, and V. M. N. Passaro, "Design of an exceptional-surface-enhanced silicon-on-insulator optical accelerometer," *Journal of Lightwave Technology*, vol. 39, no. 18, pp. 5954–5961, Sep. 2021. [Online]. Available: https://doi.org/10.1109/jlt.2021.3091333

[32] M. De Carlo, "Exceptional points of parity-time- and anti-parity-time-symmetric devices for refractive index and absorption-based sensing," *Results in Optics*, vol. 2, p. 100052, Jan. 2021. [Online]. Available: https://doi.org/10.1016/j.rio.2020.100052

[33] H. Haus, *Waves and fields in optoelectronics*. Englewood Cliffs, NJ: Prentice-Hall, 1984.

[34] J. Wiersig, "Review of exceptional point-based sensors," *Photonics Research*, vol. 8, no. 9, p. 1457, Aug. 2020. [Online]. Available: https://doi.org/10.1364/prj.396115

[35] W. Li, H. Zhang, P. Han, X. Chang, S. Jiang, Y. Zhou, A. Huang, and Z. Xiao, "Real frequency splitting indirectly coupled anti-parity-time symmetric nanoparticle sensor," *Journal of Applied Physics*, vol. 128, no. 13, p. 134503, Oct. 2020. [Online]. Available: https://doi.org/10.1063/5.0020944

[36] B. S. Ryvkin, E. A. Avrutin, and J. T. Kostamovaara, "Strong doping of then-optical confinement layer for increasing output power of high- power pulsed laser diodes in the eye safe wavelength range," *Semiconductor Science and Technology*, vol. 32, no. 12, p. 125008, Oct. 2017. [Online]. Available: https://doi.org/10.1088/1361-6641/aa92fd

[37] J. Leuthold, M. Mayer, J. Eckner, G. Guekos, H. Melchior, and C. Zellweger, "Material gain of bulk 1.55 um InGaAsP/InP semiconductor optical amplifiers approximated by a polynomial model," *Journal of Applied Physics*, vol. 87, no. 1, pp. 618–620, Jan. 2000. [Online]. Available: https://doi.org/10.1063/1.371909